

1 **North Atlantic ocean circulation and abrupt climate change during the**  
2 **last glaciation**

3 **Authors:** L. G. Henry<sup>1\*</sup>, J. F. McManus<sup>1</sup>, W. B. Curry<sup>2,3</sup>, N. L. Roberts<sup>4</sup>, A. M.  
4 Piotrowski<sup>4</sup>, L. D. Keigwin<sup>2</sup>

5 <sup>1</sup>Lamont-Doherty Earth Observatory, Columbia University, Palisades, NY 10964 USA.

6 <sup>2</sup>Woods Hole Oceanographic Institution, Woods Hole, MA 02543. USA

7 <sup>3</sup>Bermuda Institute of Ocean Sciences, St. George's, Bermuda.

8 <sup>4</sup>University of Cambridge, Department of Earth Sciences, Cambridge UK CB2 3EQ

9 \*Author to whom correspondence should be addressed ([lhenry@ldeo.columbia.edu](mailto:lhenry@ldeo.columbia.edu))

10

11 **The last ice age was characterized by rapid and hemispherically asynchronous**  
12 **climate oscillations, whose origin remains unresolved. Variations in oceanic**  
13 **meridional heat transport may contribute to these repeated climate changes, which**  
14 **were most pronounced during the glacial interval twenty-five to sixty thousand**  
15 **years ago known as marine isotope stage 3 (MIS3). Here we examine a sequence of**  
16 **climate and ocean circulation proxies throughout MIS3 at high resolution in a deep**  
17 **North Atlantic sediment core, combining the kinematic tracer Pa/Th with the most**  
18 **widely applied deep water-mass tracer,  $\delta^{13}\text{C}_{\text{BF}}$ . These indicators reveal that Atlantic**  
19 **overturning circulation was reduced during every cool northern stadial, with the**  
20 **greatest reductions during episodic iceberg discharges from the Hudson Strait, and**  
21 **that sharp northern warming followed reinvigorated overturning. These results**  
22 **provide direct evidence for the ocean's persistent, central role in abrupt glacial**  
23 **climate change.**

24

25 **One Sentence Summary:** Multiple proxies reveal that ocean circulation changes  
26 accompanied and preceded each millennial climate oscillation within marine isotope  
27 stage 3 (MIS 3) of the last ice age, 60ka to 25ka.

28

29 Unlike the relatively stable preindustrial climate of the past ten thousand years,  
30 glacial climate was characterized by repeated millennial oscillations (1). These  
31 alternating cold stadial and warm interstadial events were most abrupt and pronounced on  
32 Greenland and across much of the northern hemisphere, with the most extreme regional  
33 conditions during several Heinrich (H) events (2), catastrophic iceberg discharges into the  
34 subpolar North Atlantic Ocean. These abrupt events not only had impact on global  
35 climate, but also are associated with widespread reorganizations of the planet's  
36 ecosystems(3). Geochemical fingerprinting of the ice rafted detritus (IRD) associated  
37 with the most pronounced of these events consistently indicates a source in the Hudson  
38 Strait (HS) (4), so we abbreviate this subset of H events as HS events and their following  
39 cool periods as HS stadials. During northern stadials, ice cores show that Antarctica  
40 warmed, and each subsequent rapid northern hemisphere warming was followed shortly  
41 by cooling at high southern latitudes (5). Explanations for the rapidity and asynchrony of  
42 these climate changes require a mechanism for partitioning heat on a planetary scale,  
43 initiated either through reorganization of atmospheric structure (6) or the ocean's  
44 thermohaline circulation, particularly the Atlantic meridional overturning circulation  
45 (AMOC) (7-10). Coupled climate models have successfully used each of these  
46 mechanisms to generate time series that replicate climate variability observed in  
47 paleoclimate archives (9, 11). Here we investigate the relationship between Northern

48 Hemispheric climate as recorded in Greenland ice cores and marine sediments, along  
49 with isotopic deep-sea paleoproxies sensitive to changes in North Atlantic Deep Water  
50 (NADW) production and AMOC transport during Marine Isotope Stage 3 (MIS3).  
51 Throughout that time, when climate was neither as warm as today nor as cold as the last  
52 glacial maximum (LGM), ice sheets of intermediate size blanketed much of the northern  
53 hemisphere, and large millennial stadial - interstadial climate swings (6, 8) provide a  
54 wide dynamic range that allows examination of the ocean's role in abrupt change.

55 Sediment samples were taken from the long (35m) core KNR191-CDH19,  
56 recovered from the Bermuda Rise (33° 41.443' N; 57° 34.559' W, 4541m water depth) in  
57 the northwestern Atlantic Ocean (Fig. 1), near previous seafloor sampling at Integrated  
58 Ocean Drilling Program (IODP) site 1063, and coring sites KNR31 GPC-5, EN120 GGC-  
59 1, MD95-2036, and others. Because this region of the deep North Atlantic is  
60 characterized by steep lateral gradients in tracers of NADW and Antarctic Bottom Water  
61 (AABW), the Bermuda Rise has been intensively used to explore the connection between  
62 changes in ocean circulation and climate (7, 12). In this study we measured the  
63 radioisotopes  $^{231}\text{Pa}$  and  $^{230}\text{Th}$  in bulk sediment, age-corrected to the time of deposition,  
64 along with stable carbon ( $\delta^{13}\text{C}$ ) and oxygen ( $\delta^{18}\text{O}$ ) isotope ratios in the microfossil shells  
65 of both epibenthic foraminifera (*Cibicidoides wuellerstorfi* and *Nuttallides umbonifera*)  
66 and planktonic foraminifera (*Globergerinoides ruber*) respectively, yielding inferences  
67 on relative residence times and the origin of deep water masses on centennial time scales.

68 The isotopes  $^{231}\text{Pa}$  and  $^{230}\text{Th}$  are produced from the decay of  $^{235}\text{U}$  and  $^{234}\text{U}$ ,  
69 respectively, dissolved in seawater. This activity of  $^{231}\text{Pa}$  and  $^{230}\text{Th}$  in excess of the  
70 amount supported by the decay of uranium within the crystal lattice of the sediment's

71 mineral grains is denoted by  $^{231}\text{P}_{\text{xs}}$  and  $^{230}\text{Th}_{\text{xs}}$ . As the parent U isotopes have long  
72 residence times, U is well mixed throughout the ocean. This yields a  $^{231}\text{Pa}_{\text{xs}}/^{230}\text{Th}_{\text{xs}}$   
73 (hereafter Pa/Th) production ratio (Pa/Th = 0.093) that is constant and uniformly  
74 distributed (13, 14). Both daughter isotopes are removed by adsorption onto settling  
75 particles, with Th more efficiently scavenged than Pa. The residence time of  $^{231}\text{Pa}_{\text{xs}}$  ( $\tau_{\text{res}}$   
76  $\approx$  200yr) in seawater is thus greater than that of  $^{230}\text{Th}_{\text{xs}}$  ( $\tau_{\text{res}} \approx$  30yr), allowing  $^{231}\text{Pa}_{\text{xs}}$  to  
77 be redistributed laterally by changes in basin-scale circulation before deposition (7, 14-  
78 16), with the additional potential influence of removal due to changes in particle rain  
79 associated with biological productivity (17). Settling particles (18) and surface sediments  
80 throughout the basin reveal a deficit in  $^{231}\text{Pa}_{\text{xs}}$  burial that is consistent with large-scale  
81 export by the deep circulation (Fig. 1 and supplemental discussion).

82         The downcore Pa/Th in core CDH-19 ranges from  $\sim$ 0.05 to slightly above the  
83 production ratio of 0.093, with a series of well-defined variations throughout MIS 3  
84 (Fig.2). In sediments deposited during Greenland interstadial intervals(1), Pa/Th ratios  
85 average  $0.0609 \pm 0.0074$  ( $2\sigma$ ), substantially below the production ratio (Fig. 2), and only  
86 10% higher than the mean value (Pa/Th = 0.055) of the Holocene, a time of relatively  
87 vigorous AMOC (7). Because  $^{230}\text{Th}_{\text{xs}}$  is buried in near balance with its production (19),  
88 the relatively low Pa/Th indicates a substantial lateral export of  $^{231}\text{Pa}_{\text{xs}}$ , consistent with  
89 relatively vigorous AMOC during interstadials, although the vertical integration through  
90 the water column of this deficit does not distinguish whether this export occurred at deep  
91 or intermediate levels. Epibenthic  $\delta^{13}\text{C}$  ( $\delta^{13}\text{C}_{\text{BF}}$ ) data allow discrimination between these  
92 two possibilities, and display increased values during each interstadial, implying a greater  
93 contribution of the isotopically more positive North Atlantic end member (Fig 2). During

94 these intervals, this positive isotopic signal suggests a deeper overturning cell was  
95 established, rather than a shallower, yet vigorous one. This confirms a previous  
96 suggestion of intervals of relatively strong AMOC within the last ice age (20, 21),  
97 although neither Pa/Th nor  $\delta^{13}\text{C}_{\text{BF}}$  adjusted for whole ocean inventory changes (Curry  
98 and Oppo, 2005XXX) reach early Holocene values.

99 Pa/Th increases within each Greenland stadial interval, for a mean duration of  
100 0.531 +/- 0.303ka to a Pa/Th value of 0.0797+/-0.0154, indicating decreased lateral  
101 export of  $^{231}\text{Pa}_{\text{XS}}$  and consistent with a shallower or reduced overturning cell in the North  
102 Atlantic. During these stadials,  $\delta^{13}\text{C}_{\text{BF}}$  decreases significantly to negative values (-0.2‰  
103 to -0.5‰), suggesting greater influence of the glacial equivalent of modern Antarctic  
104 Bottom Water (AABW), an isotopic result consistent with reduced AMOC from a  
105 coupled climate model (10). Although the northern and southern water mass end  
106 members are not well known throughout the last glaciation, deep waters in the Atlantic  
107 during the LGM ranged from less than -0.5‰ in the south to more than 1.5‰ in the north  
108 (22). If these values prevailed throughout MIS 3, then the low benthic  $\delta^{13}\text{C}_{\text{BF}}$  indicates a  
109 dominant stadial influence of southern waters, and substantial northward retreat or  
110 shoaling of the AABW/NADW mixing zone, which is consistent with the deep water  
111 mass configuration that has previously been reconstructed for the LGM (22, 23), although  
112 not for millennial-scale stadial intervals within the glaciation.

113 The mean Pa/Th of both stadials and interstadials is consistent with export of  
114  $^{231}\text{Pa}_{\text{XS}}$  from the subtropical North Atlantic during all of MIS3. During peak interstadials,  
115 when low Pa/Th indicates the local burial of approximately half of  $^{231}\text{Pa}_{\text{XS}}$  production, the  
116 remaining half would have been exported. In contrast, the substantial decrease in the

117 lateral export of  $^{231}\text{Pa}_{\text{xs}}$  evident in higher Pa/Th, along with lower benthic  $\delta^{13}\text{C}_{\text{BF}}$  during  
118 each stadial interval, points to repeated reductions in AMOC and its attendant northward  
119 heat transport throughout MIS3. The contrast between apparent deep, vigorous  
120 overturning during interstadials, with shallower(24), weaker overturning during stadials,  
121 is most pronounced in conjunction with all HS stadials (Fig. 2), when catastrophic  
122 discharge of melting icebergs from Canada flooded the subpolar North Atlantic (4).

123 Sediments deposited during HS stadials are characterized by a mean duration of  
124 1.65 +/- 0.545ka and an average Pa/Th of 0.095 +/- 0.016, which is indistinguishable  
125 from the production ratio. These results therefore indicate no net export of  $^{231}\text{Pa}_{\text{xs}}$  from  
126 the subtropical North Atlantic during these events sourced from the Hudson Strait. This  
127 balance between seawater radiometric production and underlying sedimentary burial  
128 would be expected under conditions with a substantial reduction in AMOC or other  
129 lateral transport, and might imply a near cessation of  $^{231}\text{Pa}_{\text{xs}}$  export through deep  
130 circulation. Although variable scavenging may also contribute to sedimentary Pa/Th,  
131 values throughout MIS 3 bear only a weak relationship with bulk and opal fluxes ( $r^2=0.19$ ,  
132 S2), which therefore constitute secondary influences.

133

134 These new results reveal that AMOC variations were associated with every MIS 3  
135 stadial-interstadial oscillation, with the largest reductions during HS stadials. The well-  
136 resolved interval 35-50 ka provides a good example (Fig. 3). This iconic interval contains  
137 H4, H5, and the intervening series of oscillations that have served as a basis for  
138 conceptual and computer models seeking to explain such variability (8-11, 25, 26). A  
139 previous Pa/Th record (20) covering this interval captured much of the overall amplitude,

140 and the new data resolve each stadial increase in Pa/Th, indicating that only HS4 and  
141 HS5 reach the production ratio of 0.093. Because the interstadial values are similar to  
142 each other, the subsequent abrupt increases in AMOC and regional warming are also the  
143 greatest, and occur within the century-scale response time of Pa/Th. Throughout the  
144 records, the Pa/Th and  $\delta^{13}\text{C}_{\text{BF}}$  bear a striking similarity to model output forced by  
145 freshwater anomalies (11).

146 Combined with previous investigations (7, 27), these new results confirm that all  
147 HS events of the past 60kyr were associated with a dramatic increase in Pa/Th, and are  
148 evidence for major reduction in AMOC in association with the largest IRD events (28).  
149 In contrast, H3, the sole Heinrich event stadial that fails to reach the production ratio  
150 (peak Pa/Th = 0.079), displays smaller IRD fluxes across the subpolar Atlantic (28) with  
151 provenance inconsistent with a Hudson Strait source (4). This muted result for H3 is  
152 consistent with evidence from the Florida Straits (29) showing a smaller reduction at that  
153 time in the northward flow of near-surface waters that feed the overturning circulation.  
154 As with all stadials, the HS events are characterized by lower  $\delta^{13}\text{C}_{\text{BF}}$ , suggesting  
155 diminished influence of NADW and proportionately greater AABW on Bermuda Rise.  
156 Combined Pa/Th and  $\delta^{13}\text{C}_{\text{BF}}$  results therefore indicate a persistent pattern of stadial  
157 weakening and interstadial strengthening, with a repeatedly largest reduction in AMOC  
158 associated with all HS events. Although these observations are consistent with a number  
159 of numerical model simulations (11, 26) as well as conceptual models for the  
160 mechanisms of abrupt change, they have previously been difficult to document and fully  
161 resolve (20).

162           Recent data from the Western Antarctic ice sheet provide compelling evidence for  
163 a robust lead of Greenland climate over Antarctica (5). That analysis revealed a N.  
164 Hemisphere lead of 208 +/-96 years, indicating that the interhemispheric teleconnection  
165 propagates from north to south on timescales consistent with basin-scale ocean  
166 circulation. To ascertain whether Northern Hemisphere climate is forced or reinforced by  
167 changes in AMOC, we investigated the phase relationship between surface and deep-sea  
168 properties. Cross-correlations were performed on each of  $\delta^{13}\text{C}_{\text{BF}}$ , Pa/Th, SST,  $\text{CaCO}_3$   
169 with NGRIP  $\delta^{18}\text{O}$  from both sediment cores CDH19 and MD95-2036 from the Bermuda  
170 Rise. The optimal correlation of  $\delta^{13}\text{C}_{\text{BF}}$  leads NGRIP  $\delta^{18}\text{O}$  by approximately two  
171 centuries (Fig 4). This lead is corroborated by Pa/Th phasing which, when considering  
172 the century-scale response time of the proxy (13, 14), is consistent with AMOC changes  
173 indicated by  $\delta^{13}\text{C}_{\text{BF}}$ . The SST reconstruction from MD95-2036 was aligned with  
174 Greenland  $\delta^{18}\text{O}$ , yielding a correlation of  $r^2=0.83(30)$ . SST and Pa/Th are synchronous  
175 with NGRIP to within the estimated bioturbation error of 8cm within the core, displaying  
176 correlations with Greenland of  $r^2=0.47$  for Pa/Th, and  $r^2=0.65$  for SST. The optimal  
177 correlation of  $\% \text{CaCO}_3$ ,  $r^2=0.64$ , lags NGRIP  $\delta^{18}\text{O}$  by nearly 200 years.

178           The consistent lead of variations in  $\delta^{13}\text{C}_{\text{BF}}$  before SST and Greenland  
179 temperatures, repeated over multiple millennial cycles, indicates the potential influence  
180 of AMOC on NH climate, and suggests the Bermuda Rise is exposed to shifts in deep  
181 water mass mixing. Initially, deep circulation changes, evidenced overall by the timing of  
182  $\delta^{13}\text{C}_{\text{BF}}$ . Pa/Th shifts essentially in tandem with regional temperature when circulation  
183 accelerates, and soon thereafter as it responds to weakening AMOC (S3). Given the  
184 response time of Pa/Th to instantaneous shifts in North Atlantic overturning(13, 14), this



185 also suggests that changes in AMOC precede regional temperature change, although the  
186 exact timing may have differed during cooling and warming phases. Both SST and  
187 Greenland temperature proxies lag the ocean circulation in a consistent fashion, and in  
188 turn these northern changes have been demonstrated to lead Antarctic temperatures (5).  
189 Calcium-carbonate concentration is the last of the proxies to respond to AMOC change,  
190 consistent with the longer timescale of preservation, dissolution and dilution in the deep  
191 ocean.

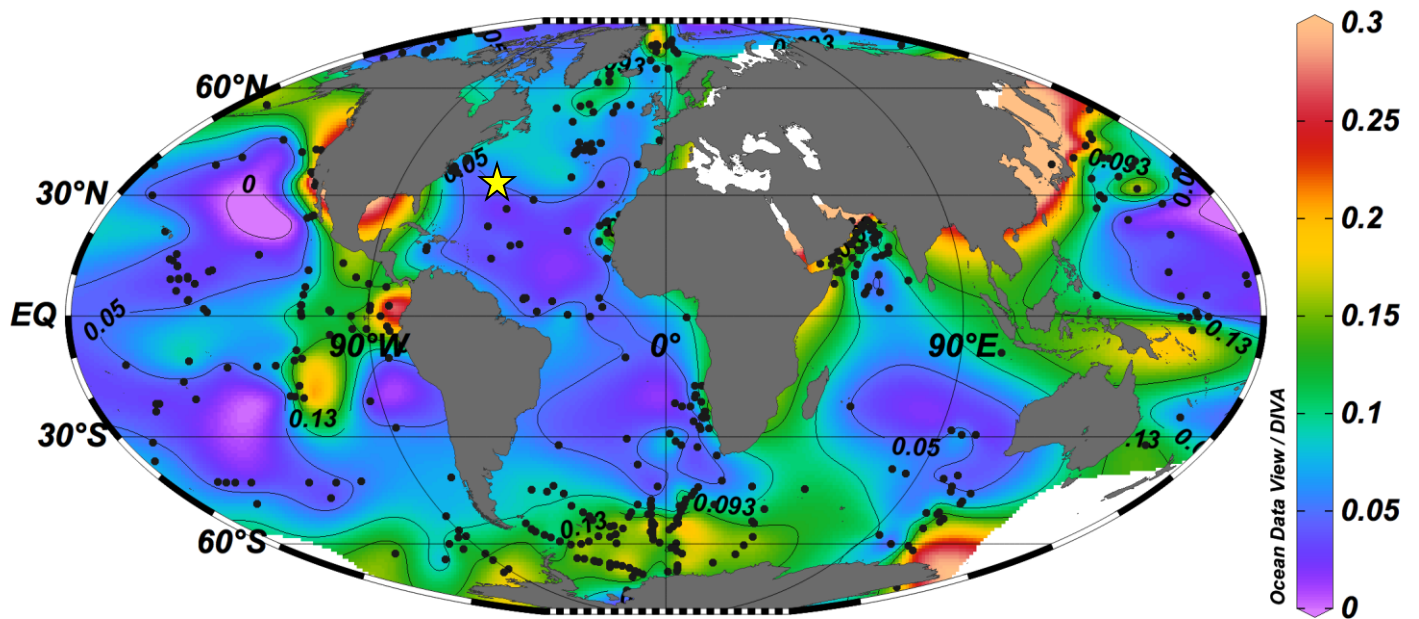
192         The relative timing of the observed AMOC changes has important implications  
193 for regional and global climate. While numerous computer simulations suggest that  
194 melting icebergs and other freshwater input associated with H events may have shut  
195 down NADW production(9, 11, 26), recent results examining the phasing of North  
196 Atlantic SST and ice rafted detritus (IRD) suggest stadial conditions began to develop  
197 prior to ice-rafting(31). The evidence here nevertheless indicates that the greatest AMOC  
198 reduction and the coldest stadial intervals accompanied the largest iceberg discharges.  
199 This suggests that the iceberg discharges may have provided a positive feedback  
200 mechanism to accelerate the initial cooling within each multi millennial climate cycle. In  
201 addition, the extended Heinrich-stadial reductions in AMOC observed in this study  
202 coincide with intervals of rising atmospheric CO<sub>2</sub>(32), while CO<sub>2</sub> declined when AMOC  
203 increased during the subsequent sharp transitions to northern interstadials, supporting a  
204 potential influence on the atmosphere by the deep circulation on millennial  
205 timescales(33).

206

207           The robust relationship of reductions in export of northern deep waters evident in  
208 reduced  $^{231}\text{Pa}_{\text{xs}}$  export and decreased  $\delta^{13}\text{C}_{\text{BF}}$  before and during stadial periods, and the  
209 dramatic increases in both during interstadials provides direct evidence for the role of  
210 AMOC in abrupt glacial climate change. The sequence of marked circulation changes  
211 and northern hemisphere climate detailed here, combined with the demonstrated lag of  
212 Antarctic temperature variations (5), strongly implicates changes in meridional heat  
213 transport by the ocean as a trigger for abrupt northern hemisphere warming and the  
214 tipping of the “bipolar seesaw (25).”

215  
216  
217  
218  
219  
220  
221  
222  
223  
224  
225

Figures



226

227

228

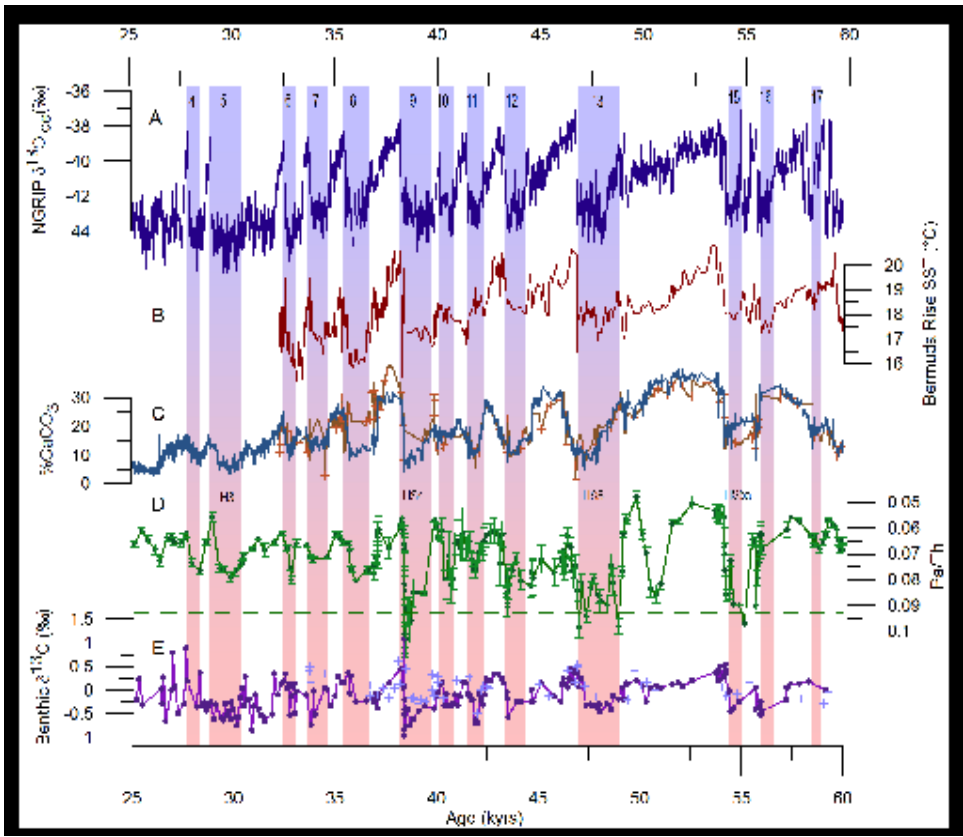
229

230

231 **Fig. 1.** Location sediment core CDH19 shown as star ( $33^{\circ} 41.443' N$ ;  $57^{\circ} 34.559' W$ ,  
 232 4541m water depth) with Pa/Th ratios (black dots) in core top sediments used with ODV  
 233 DIVA gridding to produce the color contours.

234

235



236

237

238

239

240

241

242

243

244

245

246

247

248

249

250

251

252 **Fig. 2.** Stadials are numbered with vertical bars. [A] NGRIP ice core  $\delta^{18}\text{O}_{\text{ice}}$   
253 75.1°N, 42.32°W (34). [B] SST (°C) from MD95-2036, 33° 41.444'N, 57° 34.548'W,  
254 4462m (30). [C] Calcium x-ray fluorescence (orange) from core CDH19 (this study)  
255 mapped to %CaCO<sub>3</sub>, with calibration  $r^2 = 0.87$  (S.1), with spectral reflectance (blue) from  
256 core MD95-2036 (35) [D] Pa/Th from bulk sediment (green) taken from core CDH19.  
257 [G] Benthic foraminiferal  $\delta^{13}\text{C}_{\text{BF}}$  from core CDH19 (purple) alternates between values  
258 consistent with southern and northern sourced  $\delta^{13}\text{C}_{\text{BF}}$  end members.

259

260

261

262

263

264

265

266

267

268

269

270

271

272

273

274

275

276

277

278

279

280

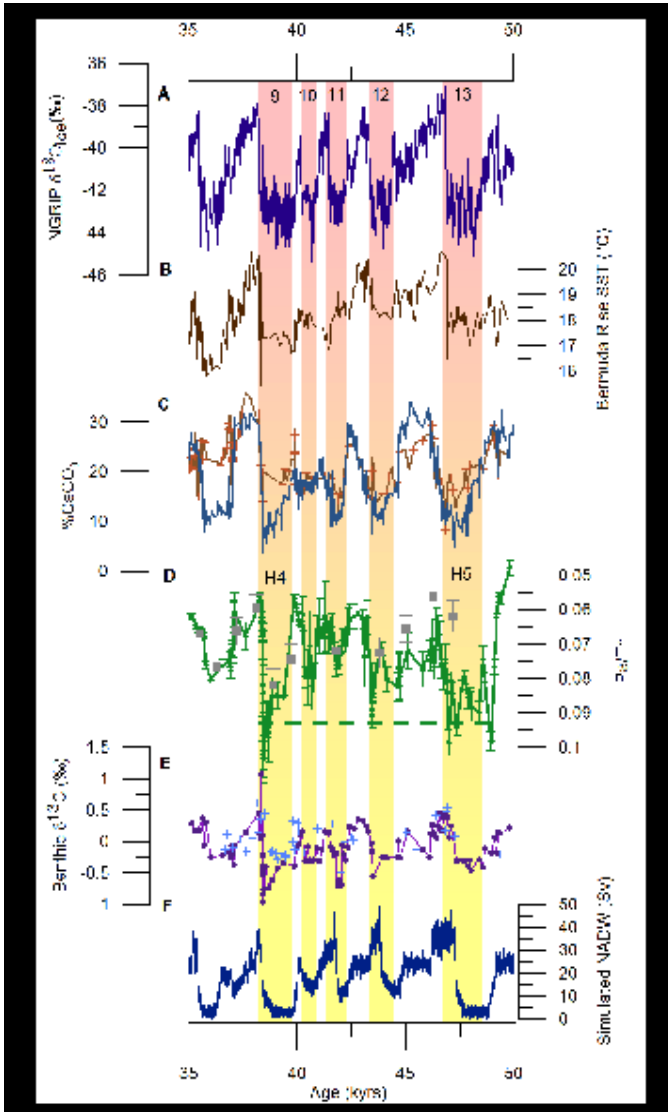
281

282

283

284

285  
286  
287  
288  
289



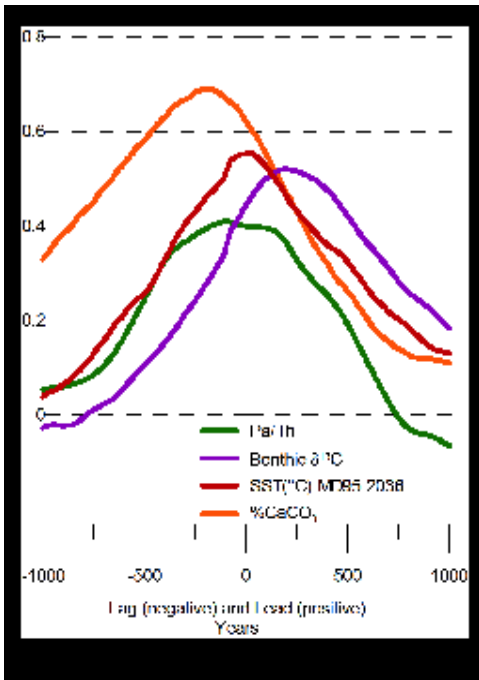
290  
291  
292  
293  
294  
295  
296  
297  
298  
299  
300  
301

302  
303  
304  
305  
306  
307  
308  
309  
310  
311  
312  
313  
314  
315  
316  
317  
318  
319  
320  
321  
322  
323  
324  
325  
326  
327

**Fig. 3.** (A) through (E) as in Figure 2, with the addition of (F) simulated NADW (Sv) in a coupled ocean/atmosphere model (11), with previously published Böhm et al Pa/Th data (20) and Keigwin and Boyle  $\delta^{13}\text{C}_{\text{BF}}$  data (12).

328

329



330

331

332

333

334

335

336

337

338

339

340

341

342

343

344

345

346

347

348

349

350

351

352

353



354

355

356

357

358 **Fig. 4.** Correlation of NGRIP ice core  $\delta^{18}\text{O}$  with CDH19  $\text{CaCO}_3$  flux (blue), Pa/Th of

359 bulk sediment from CDH19 (green),  $\delta^{13}\text{C}_{\text{BF}}$  from CDH19 (purple), SST  $^{\circ}\text{C}$  from MD95-

360 2036 (30) (red).

361

362

363

364

365

366

367

368

369

370

371

372

373

374

375

376

377

378

379

380

381

382

383

384

385

386

387 References and Notes

- 388 1. W. Dansgaard, S. Johnsen, H. Clausen, Evidence for general instability of past  
389 climate from a 250-kyr ice-core record. *Nature*. **364**, 218–220 (1993).
- 390 2. W. Broecker, G. Bond, M. Klas, E. Clark, J. McManus, Origin of the northern  
391 Atlantic's Heinrich events. *Climate Dynamics*. **6**, 265–273 (1992).
- 392 3. M. Yasuhara, T. M. Cronin, P. B. Demenocal, H. Okahashi, B. K. Linsley, Abrupt  
393 climate change and collapse of deep-sea ecosystems. *Proceedings of the National  
394 Academy of Sciences of the United States of America*. **105**, 1556–1560 (2008).
- 395 4. S. R. Hemming, Heinrich events: Massive late Pleistocene detritus layers of the  
396 North Atlantic and their global climate imprint. *Rev. Geophys.* **42** (2004).
- 397 5. C. Buizert *et al.*, Precise inter-polar phasing of abrupt climate change during the  
398 last ice age. *Nature*. **520**, 661–665 (2015).
- 399 6. X. Zhang, G. Lohmann, G. Knorr, C. Purcell, Abrupt glacial climate shifts  
400 controlled by ice sheet changes. *Nature*. **512**, 290–294 (2014).
- 401 7. J. McManus, R. Francois, J. M. Gherardi, L. Keigwin, S. Brown-Leger, Collapse  
402 and rapid resumption of Atlantic meridional circulation linked to deglacial climate  
403 changes. *Nature*. **428**, 834–837 (2004).
- 404 8. R. B. Alley, P. Clark, L. Keigwin, R. Webb, Making sense of millennial-scale  
405 climate change. *Geophysical Monograph Series*. **112**, 385–394 (1999).

- 406 9. S. Rahmstorf, Ocean circulation and climate during the past 120, 000 years. *Nature*.  
407 **419**, 207–214 (2002).
- 408 10. A. Schmittner, D. C. Lund, Early deglacial Atlantic overturning decline and its  
409 role in atmospheric CO<sub>2</sub> rise inferred from carbon isotopes  
410 ( $\delta^{13}\text{C}$ ). *Climate of the Past*. **11**, 135–152 (2015).
- 411 11. L. Menviel, A. Timmermann, T. Friedrich, Hindcasting the continuum of  
412 Dansgaard-Oeschger variability: mechanisms, patterns and timing. *Climate of the*  
413 *Past* (2013).
- 414 12. L. Keigwin, E. Boyle, Surface and deep ocean variability in the northern Sargasso  
415 Sea during marine isotope stage 3. *Paleoceanography* (1999).
- 416 13. G. M. Henderson, R. F. Anderson, The U-series toolbox for paleoceanography.  
417 *Reviews in mineralogy and geochemistry*. **52**, 493 (2003).
- 418 14. E. F. Yu, R. Francois, M. P. Bacon, Similar rates of modern and last-glacial ocean  
419 thermohaline circulation inferred. *Nature*. **379**, 22 (1996).
- 420 15. C. Negre *et al.*, Reversed flow of Atlantic deep water during the Last Glacial  
421 Maximum. *Nature*. **468**, 84–88 (2010).
- 422 16. J. M. Gherardi *et al.*, Glacial-interglacial circulation changes inferred from <sup>231</sup>Pa/  
423 <sup>230</sup>Th sedimentary record in the North Atlantic region. *Paleoceanography*. **24**  
424 (2009).
- 425 17. R. F. Anderson *et al.*, Wind-Driven Upwelling in the Southern Ocean and the  
426 Deglacial Rise in Atmospheric CO<sub>2</sub>. *Science*. **323**, 1443–1448 (2009).
- 427 18. C. Hayes, R. F. Anderson, M. Fleisher, S. Vivancos, Intensity of Th and Pa  
428 scavenging partitioned by particle chemistry in the North Atlantic Ocean. *Marine*  
429 *Chemistry*. **170**, 49–60 (2015).
- 430 19. G. M. Henderson, C. Heinze, R. F. Anderson, A. M. E. Winguth, Global  
431 distribution of the <sup>230</sup>Th flux to ocean sediments constrained by GCM modelling.  
432 *Deep Sea Research Part I: Oceanographic Research Papers*. **46**, 1861–1893  
433 (1999).
- 434 20. E. Böhm *et al.*, Strong and deep Atlantic meridional overturning circulation during  
435 the last glacial cycle. *Nature*. **517**, 73–76 (2014).
- 436 21. J. Gottschalk *et al.*, Abrupt changes in the southern extent of North Atlantic Deep  
437 Water during Dansgaard–Oeschger events. *Nature Geosci*. **8**, 950–954 (2015).
- 438 22. W. B. Curry, D. W. Oppo, Glacial water mass geometry and the distribution of  $\delta$   
439 <sup>13</sup>C of  $\Sigma\text{CO}_2$  in the western Atlantic Ocean. *Paleoceanography*. **20** (2005).

- 440 23. J. F. Adkins, The role of deep ocean circulation in setting glacial climates.  
441 *Paleoceanography*. **28**, 539–561 (2013).
- 442 24. R. Zahn, A. Stüber, Suborbital intermediate water variability inferred from paired  
443 benthic foraminiferal Cd/Ca and  $\delta^{13}\text{C}$  in the tropical West Atlantic and linking  
444 with North Atlantic climates. *Earth and Planetary Science Letters*. **200**, 191–205  
445 (2002).
- 446 25. W. Broecker, Paleocean circulation during the last deglaciation: a bipolar seesaw?  
447 *Paleoceanography*. **13**, 119–121 (1998).
- 448 26. A. Ganopolski, S. Rahmstorf, Rapid changes of glacial climate simulated in a  
449 coupled climate model. *Nature*. **409**, 153–158 (2001).
- 450 27. J. Lippold *et al.*, Does sedimentary  $^{231}\text{Pa}/^{230}\text{Th}$  from the Bermuda Rise monitor  
451 past Atlantic Meridional Overturning Circulation? *Geophys. Res. Lett.* **36** (2009).
- 452 28. J. F. McManus, R. F. Anderson, W. S. Broecker, M. Q. Fleisher, S. M. Higgins,  
453 Radiometrically determined sedimentary fluxes in the sub-polar North Atlantic  
454 during the last 140,000 years. *Earth and Planetary Science Letters*. **155**, 29–43  
455 (1998).
- 456 29. J. Lynch-Stieglitz, M. Schmidt, L. Henry, W. B. Curry, Muted change in Atlantic  
457 overturning circulation over some glacial-aged Heinrich events. *Nature Geosci.* **7**,  
458 144–150 (2014).
- 459 30. J. P. Sachs, Subtropical North Atlantic Temperatures 60,000 to 30,000 Years Ago.  
460 *Science*. **286**, 756–759 (1999).
- 461 31. S. Barker *et al.*, Icebergs not the trigger for North Atlantic cold events. *Nature*.  
462 **520**, 333–336 (2015).
- 463 32. J. S. Ahn, E. J. Brook, Atmospheric CO<sub>2</sub> and Climate on Millennial Time Scales  
464 During the Last Glacial Period. *Science*. **322**, 83–85 (2008).
- 465 33. A. Schmittner, E. D. Galbraith, Glacial greenhouse-gas fluctuations controlled by  
466 ocean circulation changes. *Nature*. **456**, 373–376 (2008).
- 467 34. A. Svensson *et al.*, A 60 000 year Greenland stratigraphic ice core chronology.  
468 *Climate of the Past*. **4**, 47–57 (2008).
- 469 35. E. Boyle, (1997), vol. 94, pp. 8300–8307.
- 470
- 471
- 472

473

474

475

476

477 Acknowledgements

478

479

480 Data will be made available at <http://nsidc.org/data/> and <http://ncdc.noaa.gov/paleo/>.

481 This research was supported in part by a NSF Graduate Research Fellowship to L.G.H,

482 by awards from the Comer Science and Education Foundation and NSF ATM-0936496 to

483 J.F.M., and an award from the LDEO Climate Center to L.G.H. and J.F.M. LDK and

484 WBC were supported by ATM-0836472, and LDK was supported by AGS 1548160. We

485 thank M. Jeglinski and K. Rose for technical support. The authors would like to thank

486 Robert Anderson, Sidney Hemming and Christopher Hayes for constructive discussion

487 leading to improvement of the manuscript, and Martin Fleisher for analytical support.

488

489